

Quantum scars from zero modes in an Abelian lattice gauge theory on ladders

Debasish Banerjee^{1,2} and Arnab Sen³

¹*Institut für Physik, Humboldt-Universität zu Berlin,
Zum Großen Windkanal 6, 12489 Berlin, Germany*

²*Saha Institute of Nuclear Physics, HBNI, 1/AF Bidhannagar, Kolkata 700064, India*

³*School of Physical Sciences, Indian Association for the Cultivation of Science, Kolkata 700032, India*

We consider the spectrum of a $U(1)$ quantum link model where gauge fields are realized as $S = 1/2$ spins and demonstrate a new mechanism for generating quantum many-body scars (high-energy eigenstates that violate the eigenstate thermalization hypothesis) in a constrained Hilbert space. Many-body dynamics with local constraints has attracted much attention due to the recent discovery of non-ergodic behavior in quantum simulators based on Rydberg atoms. Lattice gauge theories provide natural examples of constrained systems since physical states must be gauge-invariant. In our case, the Hamiltonian $H = \mathcal{O}_{\text{kin}} + \lambda \mathcal{O}_{\text{pot}}$, where \mathcal{O}_{pot} (\mathcal{O}_{kin}) is diagonal (off-diagonal) in the electric flux basis, contains exact mid-spectrum zero modes at $\lambda = 0$ whose number grows exponentially with system size. This massive degeneracy is lifted at any non-zero λ but some special linear combinations that simultaneously diagonalize \mathcal{O}_{kin} and \mathcal{O}_{pot} survive as quantum many-body scars, suggesting an “order-by-disorder” mechanism in the Hilbert space. We give evidence for such scars and show their dynamical consequences on two-leg ladders with up to 56 spins, which may be tested using available proposals of quantum simulators. Results on wider ladders point towards their presence in two dimensions as well.

PACS numbers:

Introduction: Eigenstate thermalization hypothesis (ETH) posits that individual energy eigenstates of generic many-body systems have “thermal” expectation values for local observables with temperature determined by the energy density of the eigenstate [1–5]. It also provides an explanation for the local equilibration of such systems under their own coherent dynamics [6, 7]. It is equally interesting to ask when this paradigm fails so that an interacting system may evade ergodicity. Two well-known mechanisms are provided by integrability [8] and many-body localization [9, 10]. In both cases, an extensive number of local integrals of motion emerge which prevents the bulk of the eigenstates from following ETH.

An important question is whether violations of ETH can occur in non-integrable systems without disorder [11]. Recently, quench experiments with a kinematically-constrained chain of 51 Rydberg atoms [12] exhibited persistent many-body revivals when initialized in a Néel state while, in contrast, other high-energy initial states thermalized rapidly. Subsequent theoretical investigations [13, 14] of a minimal model with a constrained Hilbert space to incorporate strong Rydberg blockade, the PXP model [13–16], showed this ergodicity-breaking mechanism is due to the presence of some highly athermal ETH-violating states, dubbed quantum many-body scars (QMBS), embedded in an otherwise ETH-satisfying spectrum. A flurry of theoretical research has now shown QMBS to occur in a variety of other settings [17–42] (for a review, see Ref. 43).

Constrained Hilbert spaces arise in Hamiltonian formulations of lattice gauge theories (LGTs) [44] since physical (gauge-invariant) states satisfy an appropriate Gauss law. In fact, the archetypal model for scarring in

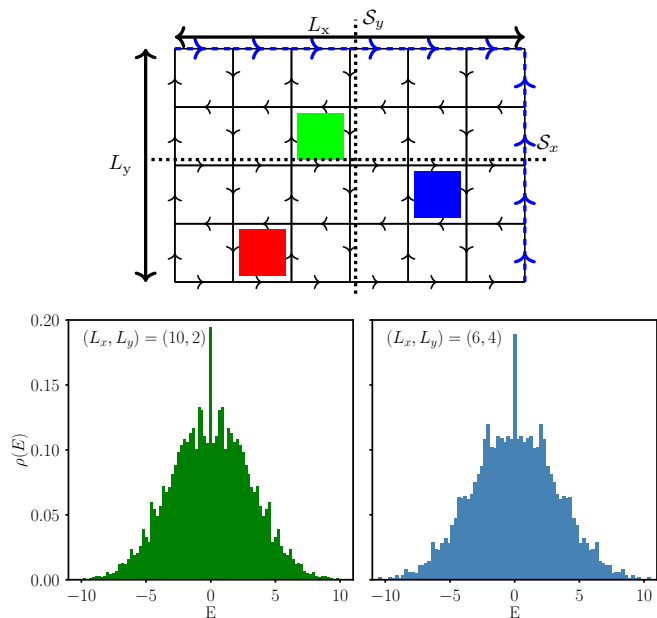


FIG. 1: (Top panel) An electric flux configuration for a ladder geometry with $(L_x, L_y) = (6, 4)$ with periodic boundary conditions in both directions. An elementary plaquette with clockwise (anticlockwise) circulation of flux is shown in blue (red) while a non-flippable plaquette is shown in green. (Bottom panel) The density of states $\rho(E)$ as a function of E for $(L_x, L_y) = (10, 2)$ (left) and $(6, 4)$ (right) at coupling $\lambda = 0$.

constrained Hilbert spaces, the PXP model, maps exactly to a lattice Schwinger model where the gauge fields are coupled with staggered fermions [45] in one dimension. Persistent oscillations starting from the Néel state then

corresponds to a string inversion [45].

It is intriguing to ask whether QMBS can appear via a completely different mechanism in other LGTs. In this Letter, we answer this question in the affirmative by considering a prototypical LGT but without any dynamical matter, a $U(1)$ quantum link model (QLM) in spin $S = 1/2$ representation [46, 47] on ladder geometries. This $U(1)$ QLM also arises as low-energy descriptions of some paradigmatic quantum spin liquids [48, 49], and displays novel crystalline confining phases [50]. We show the presence of an exponentially large number (in system size) of exact mid-spectrum zero modes in a particular limit of this LGT. Turning on another non-commuting gauge-invariant interaction lifts this massive degeneracy but also creates certain special linear combinations of these zero modes that are simultaneous eigenstates of *both* the non-commuting terms in the Hamiltonian. These QMBS are much more *localized* in the Hilbert space compared to the individual zero modes (which are delocalized) and hence the mechanism is akin to “order-by-disorder”, first introduced in the context of frustrated magnets [51, 52] (where thermal or quantum fluctuations lift the exponentially large degeneracy of classical ground states and makes the system more ordered [53, 54]), but in the Hilbert space. The number of such scars depends sensitively on the ladder geometry with striking differences between ladders of width two and four.

U(1) QLM: We consider the $U(1)$ QLM with the gauge degree of freedom being quantum spins $S = 1/2$ living on the links $\mathbf{r}, \hat{\mu}$ connecting two neighboring sites \mathbf{r} and $\mathbf{r} + \hat{\mu}$ (with $\hat{\mu} = \hat{i}, \hat{j}$) of a ladder of width L_y and length L_x (where L_x and L_y are both even), and periodic boundary conditions in both directions (Fig. 1, top panel). A $U(1)$ quantum link, $U_{\mathbf{r}, \hat{\mu}} = S_{\mathbf{r}, \hat{\mu}}^+$ is a raising operator of the electric flux $E_{\mathbf{r}, \hat{\mu}} = S_{\mathbf{r}, \hat{\mu}}^z$, and the Hamiltonian is

$$\begin{aligned} H &= \mathcal{O}_{\text{kin}} + \lambda \mathcal{O}_{\text{pot}} \\ &= - \sum_{\square} \left(U_{\square} + U_{\square}^{\dagger} \right) + \lambda \sum_{\square} \left(U_{\square} + U_{\square}^{\dagger} \right)^2, \quad (1) \end{aligned}$$

where $U_{\square} = U_{\mathbf{r}, \hat{i}} U_{\mathbf{r} + \hat{i}, \hat{j}} U_{\mathbf{r} + \hat{j}, \hat{i}}^{\dagger} U_{\mathbf{r}, \hat{j}}^{\dagger}$ and \square denotes an elementary plaquette. \mathcal{O}_{kin} acts on closed loops of electric flux around elementary plaquettes, flipping them from clockwise (anti-clockwise) to anti-clockwise (clockwise), while annihilating all other configurations. \mathcal{O}_{pot} counts the number of such flippable plaquettes. The Hamiltonian has a local $U(1)$ symmetry generated by the Gauss law $G_{\mathbf{r}} = \sum_{\mu} (E_{\mathbf{r}, \hat{\mu}} - E_{\mathbf{r} - \hat{\mu}, \hat{\mu}})$. The physical states $|\psi\rangle$ satisfy $G_{\mathbf{r}}|\psi\rangle = 0$ which implies that in- and out-going electric fluxes add up to zero at each site, thus providing a constrained Hilbert space (Fig. 1, top panel).

The spectrum of H (Eq. 1) is calculated using large-scale exact diagonalization (ED). The total electric flux winding around the lattice in a given periodic direction is a conserved quantity, related to a $U(1)$ center symmetry, and causes the Hilbert space to break

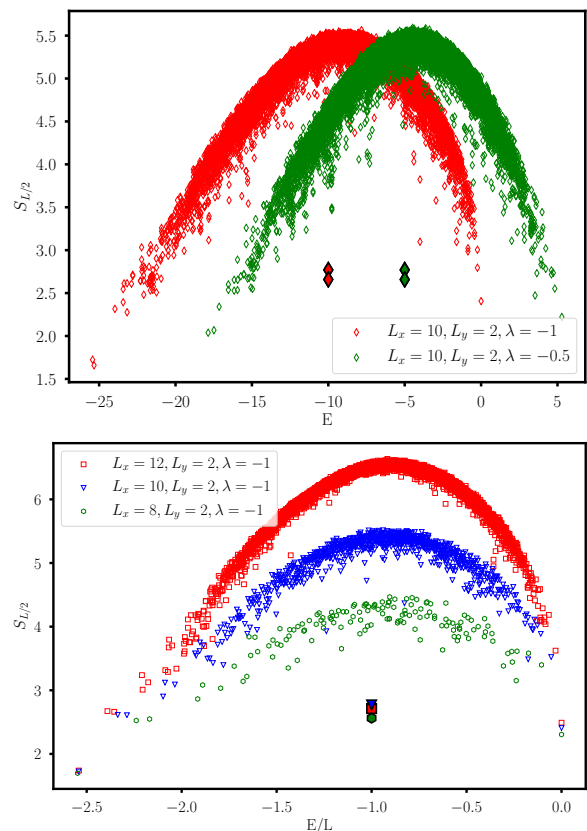


FIG. 2: The bipartite entanglement entropy with equal partitions, $S_{L/2}$, shown for all energy eigenstates of the ladder $(L_x, L_y) = (10, 2)$ at couplings $\lambda = -0.5$ (green) and $\lambda = -1$ (red) (top panel) and for ladders of width $L_y = 2$ and $L_x = 12, 10, 8$ (red, blue, green) at $\lambda = -1$ for momentum $(k_x, k_y) = (0, 0)$ (bottom panel).

up into distinct topological sectors, characterized by a pair of integer winding numbers (W_x, W_y) . We henceforth restrict ourselves to the largest such sector with $(W_x, W_y) = (0, 0)$. Furthermore, translations by one lattice spacing in both directions, point-group symmetries like appropriate 180° rotations and reflections, and charge conjugation (which reverses all electric fluxes) are discrete symmetries. These symmetries do not mutually commute and for ED, we use translation symmetry together with the $U(1)$ center symmetry to reach system sizes of up to $(L_x, L_y) = (14, 2)$ (56 spins) and $(L_x, L_y) = (8, 4)$ (64 spins) for ladders of width $L_y = 2$ and $L_y = 4$, respectively (see [55] for more details).

We calculate the bipartite entanglement entropy $S_{L/2} = -\text{Tr}[\rho_A \ln \rho_A]$ for each energy eigenstate $|\Psi\rangle$ where the reduced density matrix $\rho_A = \text{Tr}_B |\Psi\rangle\langle\Psi|$ is obtained by partitioning the ladder into two equal parts A and B (see [55] for more details), the Shannon entropy $S_1 = -\sum_{\alpha} |\psi_{\alpha}|^2 \ln |\psi_{\alpha}|^2$ where $|\Psi\rangle = \sum_{\alpha=1}^{\mathcal{N}} \psi_{\alpha} |\alpha\rangle$ when the eigenstate is expressed in a given basis $|\alpha\rangle$ with \mathcal{N} basis states and the electric flux correlator

$\frac{1}{L_x} \sum_x \langle E_j(x) E_j(x+i) \rangle$ where $E_j(x) = \sum_y E_{\mathbf{r}, \hat{j}}$. It is sufficient to study $\lambda \leq 0$ since a unitary transformation relates $H(\lambda)$ and $H(-\lambda)$ [56]. The energy level spacing distribution of the $U(1)$ QLM with weak disorder (to remove global symmetries) follows the Gaussian orthogonal ensemble prediction [57] strongly indicating that the model (Eq. 1) is non-integrable when $|\lambda| \lesssim \mathcal{O}(1)$ (see [55] for more details).

Exact zero modes at $\lambda = 0$: At $\lambda = 0$, the Hamiltonian anti-commutes with the operator $\mathcal{C} = \prod_{\mathbf{r}, \hat{\mu}} E_{\mathbf{r}, \hat{\mu}}$ where only the horizontal (vertical) links on even x (y) contribute to the product and thus each elementary plaquette contains precisely one such link. This implies that any eigenstate with energy $E \neq 0$ has a partner at $-E$ ($\mathcal{C}|E\rangle = |-E\rangle$). For any λ , H also commutes with space reflections about the axes $\mathcal{S}_x, \mathcal{S}_y$ (Fig. 1, top panel). This point-group symmetry commutes with \mathcal{C} . Remarkably, any Hamiltonian with these properties has exact zero-energy eigenstates whose number scales exponentially in the system size due to an index theorem [58]. Since the spectrum is symmetric around $E = 0$, these protected zero modes are mid-spectrum states of the Hamiltonian and not low-energy states bound to topological defects or arising from supersymmetry for which there are well-known examples [59–64]. The presence of a large number of mid-spectrum zero modes is clear from the density of states $\rho(E)$ as a function of energy E , which shows a sharp spike at $E = 0$ from the (momentum unresolved) data generated for both $(L_x, L_y) = (10, 2)$ and $(6, 4)$ (Fig. 1, bottom panel). Despite there being manifestly no level repulsion between them, the behavior of the Shannon entropy, S_1 , for the zero modes indicates that these are not anomalous when compared to other neighboring eigenstates [58] (see [55] for more details). Thus, generic linear combinations of such zero modes are expected to be delocalized in the Hilbert space and have volume-law entanglement.

QMBS at $\lambda \neq 0$: At a non-zero λ , \mathcal{C} no longer anti-commutes with the Hamiltonian and hence the manifold of zero modes is not protected and mix with the non-zero modes to form new high-energy eigenstates. The only possible exception are special linear combinations of the zero modes which are also eigenstates of \mathcal{O}_{pot} , and hence of H . Remarkably, these linear combinations also show localization in the Hilbert space and anomalously low entanglement. Such eigenstates clearly violate ETH since they remain unchanged as the coupling λ is varied in spite of the energy level spacing in their neighborhood being exponentially small in $L_x L_y$.

Ladders with $L_y = 2$: Using ED for linear dimension $8 \leq L_x \leq 14$, we show the presence of 4 QMBS, one each at momenta $(k_x, k_y) = (0, 0), (\pi, \pi), (\pi, 0)$ and $(0, \pi)$ where each of these scars is a simultaneous eigenfunction of \mathcal{O}_{pot} (with eigenvalue $N_p/2$, N_p being the total number of plaquettes) and \mathcal{O}_{kin} (with eigenvalue 0).

A defining property of QMBS is that they have a much

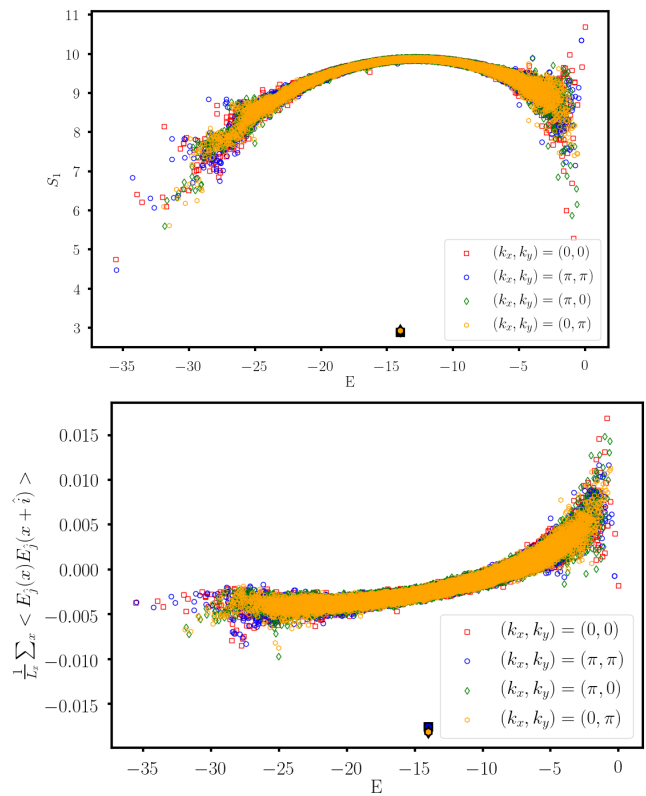


FIG. 3: The Shannon entropy, S_1 , (top panel) and the electric flux correlator (bottom panel) for all energy eigenstates of $(L_x, L_y) = (14, 2)$ at momenta $(k_x, k_y) = (0, 0), (\pi, \pi), (\pi, 0), (0, \pi)$ (shown in red, blue, green, orange) with coupling $\lambda = -1$.

lower entanglement entropy compared to their neighboring energy eigenstates and thus show up as entropy-outliers in $S_{L/2}$. This is demonstrated in the momentum-unresolved data for $S_{L/2}$ at $L_x = 10$ where the 4 QMBS are clearly visible as outliers (each with a double degeneracy) at both $\lambda = -0.5$ and $\lambda = -1$ (Fig. 2, top panel). All 4 scars have the energy $E = \lambda N_p/2$. Restricting to $(k_x, k_y) = (0, 0)$ and comparing the data of $S_{L/2}$ for $L_x = 12, 10, 8$ at $\lambda = -1$ (Fig. 2, bottom panel) shows that while the other mid-spectrum eigenstates seem to follow a volume law scaling for $S_{L/2}$ as expected from ETH, the scar state has a much lower $S_{L/2}$ that scales anomalously.

Further evidence for scarring is provided by the behavior of the Shannon entropy S_1 and the electric flux correlator at $L_x = 14$. In Fig. 3 (top panel), we show the S_1 for the momentum-resolved eigenstates at momenta $(k_x, k_y) = (0, 0), (\pi, \pi), (\pi, 0)$ and $(0, \pi)$ from which it is clear that while the neighboring eigenstates with similar energies are delocalized amongst the basis states as expected of high-energy states, the 4 QMBS have a much lower S_1 indicating their localization in the Hilbert space. The electric flux correlator for the QMBS have markedly

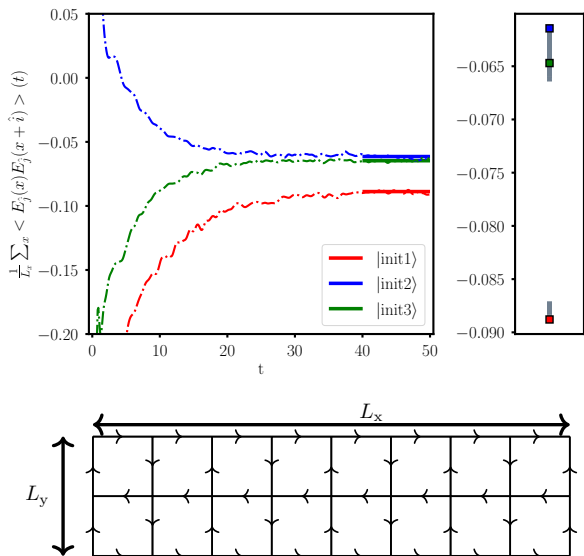


FIG. 4: (Top left panel) Unitary dynamics for $(L_x, L_y) = (14, 2)$ with three simple initial states $|\text{init}1, 2, 3\rangle$ ($|\text{init}1\rangle$ has a finite overlap with the QMBS at $(k_x, k_y) = (0, 0)$, while $|\text{init}2, 3\rangle$ has zero overlap) showing the behavior of the electric flux correlator at $\lambda = -1$ as a function of time. (Top right panel) Late-time value of the electric flux correlator for the 6433 initial states with $(k_x, k_y) = (0, 0)$ and average energy $\lambda N_p/2$ at $(L_x, L_y) = (14, 2)$. (Bottom panel) A simple reference state that generates momentum eigenstates with finite overlap with QMBS for $L_x = 8, 10, 12, 14$.

different values from the neighboring energy eigenstates (Fig. 3, bottom panel).

That special linear combinations of the exact zero modes are responsible for the creation of these QMBS can be verified by diagonalizing \mathcal{O}_{pot} only in the zero mode subspace. While most of the resulting eigenvalues are non-integers, which indicate that these states must mix with non-zero modes at finite λ (since \mathcal{O}_{pot} is a counting operator), there is one eigenvector at each of the momenta $(k_x, k_y) = (0, 0), (\pi, \pi), (\pi, 0)$ and $(0, \pi)$ with an integer eigenvalue of \mathcal{O}_{pot} that equals $N_p/2$. We have also checked that the corresponding eigenvectors have exactly the same wavefunctions as the QMBS generated at finite λ (see [55] for more details).

Expressing any of these QMBS in terms of the zero modes shows that they appear to be a pseudo-random superposition of all the zero modes (see [55] for more details). However, these states have a much smaller S_1 compared to any of the individual zero modes (see [55] for more details) showing that they are much more localized in the Hilbert space. The \mathcal{O}_{pot} term thus induces a subtle order-by-disorder mechanism in the exponentially large subspace of the zero modes to pick out a few special linear combinations and generate the QMBS at $\lambda \neq 0$.

These QMBS also leave an imprint on the unitary dynamics starting from simple high-energy initial states.

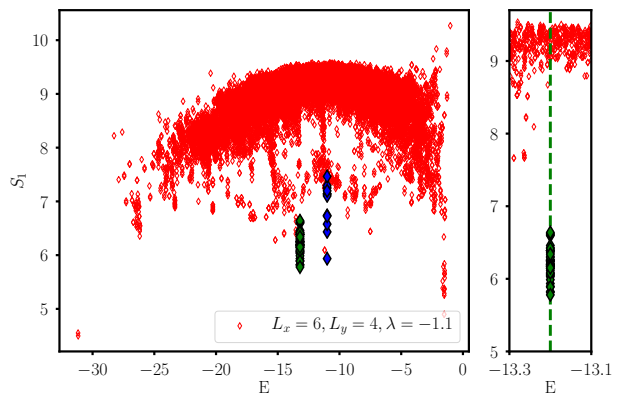


FIG. 5: (Left panel) The Shannon entropy, S_1 , for all the eigenstates for $(L_x, L_y) = (6, 4)$. The 46 (12) eigenstates with eigenvalues $(N_p/2, 0)$ ($(5N_p/12, 0)$) for $(\mathcal{O}_{\text{pot}}, \mathcal{O}_{\text{kin}})$ are shown in green (blue) for $\lambda = -1.1$. (Right panel) The same data shown in the vicinity of $E = \lambda N_p/2$ (dotted line).

Consider the class of all $(k_x, k_y) = (0, 0)$ initial states generated from any reference electric flux state with $N_p/2$ flippable plaquettes. For $(L_x, L_y) = (14, 2)$, there are 6433 such initial states with identical average energy of $\lambda N_p/2$. Out of these, only 18 initial states have a non-zero overlap with the QMBS at $(k_x, k_y) = (0, 0)$. In Fig. 4 (top left panel), we consider $\lambda = -1$ and $|\text{init}1\rangle$, an initial state with a finite overlap with the QMBS while $|\text{init}2\rangle, |\text{init}3\rangle$ have zero overlap. While the latter two initial states, even with very different starting values of the electric flux correlator, converge to very similar values at late times indicating ETH-guided thermalization, $|\text{init}1\rangle$ instead converges to a very different (subthermal) value showing that the state retains memory of its overlap with the scar at late times. The late-time value of the electric flux correlator for all these 6433 initial states (Fig. 4 (top right panel)) clearly shows that the 18 initial states with non-zero overlap with the QMBS converge to markedly different values compared to the rest. Finally, the data for $L_x = 8, 10, 12, 14$ shows that a simple initial reference state with a 2×2 unit cell (Fig. 4, bottom panel) always generates 2 momentum eigenstates with finite overlap with 2 of the QMBS (at momenta $(\pi, 0), (0, \pi)$ for $L_x = 14, 10$ and $(0, 0), (\pi, \pi)$ for $L_x = 12, 8$).

Ladders with $L_y = 4$: We consider $L_y = 4$ ladders to approach closer to the two-dimensional limit. The momentum-unresolved data for all the 32810 eigenstates at $L_x = 6$ strikingly shows that the number of QMBS is sensitive to the width of the ladder with there being 46 such anomalous eigenstates with the eigenvalue $(N_p/2, 0)$ and 12 with eigenvalue $(5N_p/12, 0)$ for $(\mathcal{O}_{\text{pot}}, \mathcal{O}_{\text{kin}})$, respectively (Fig. 5 (left panel)) (see [55] for data at $L_x = 8$ for $(k_x, k_y) = (0, 0), (\pi, \pi), (\pi, 0)$ and $(0, \pi)$ and evidence of QMBS therein). As shown in Fig. 5 (right panel), these 46 eigenstates are degenerate with $E = \lambda N_p/2$ and have a lower value of S_1 compared to that of other neighbor-

ing eigenstates which have $E \neq \lambda N_p/2$. Diagonalizing \mathcal{O}_{pot} in the zero mode subspace also yields exactly 46 (12) eigenvectors with the right integer eigenvalues $N_p/2$ ($5N_p/12$) with the other eigenvalues being non-integers.

Conclusions and outlook: We have considered a $U(1)$ QLM on finite ladders and demonstrated a new mechanism for the formation of QMBS. For the limit when the Hamiltonian only contains off-diagonal terms in the electric flux basis, there is an exponentially large (in system size) manifold of exact zero modes due to an index theorem. This massive degeneracy is lifted by applying another gauge-invariant interaction, diagonal in the electric flux basis, but some special linear combinations of the zero modes that simultaneously diagonalize both the non-commuting terms in the Hamiltonian survive and form QMBS. These also leave an imprint on the coherent dynamics of this LGT and leads to the absence of thermalization from a class of simple initial states, in particular one that can be generated from a reference state with a 2×2 unit cell. This effect can, in principle, be verified on quantum simulators based on superconducting qubits or Rydberg arrays using existing proposals [65, 66]. One possible way is to use the duality transformation to rewrite the Hamiltonian as a quantum Ising spin model. The disallowed plaquette flips can then be forbidden via Rydberg blockade to realize a gauge invariant interaction [66].

Several open issues arise from our work. Whether this mechanism survives in higher dimensions is an obvious question given our results on wider ladders. Do QMBS arise in non-Abelian QLMs is another interesting direction to explore. An analytic understanding of the algebraic properties of the zero modes and these special linear combinations is highly desirable to address whether such scarring survives in the thermodynamic limit. Finally, adding further interactions to models with an exponentially large manifold of mid-spectrum zero modes may provide yet another route to QMBS.

Acknowledgements: We thank Diptiman Sen, Krishnendu Sengupta and Uwe-Jens Wiese for useful discussions and acknowledge computational resources of DESY on the PAX cluster. We also thank Saptarshi Biswas (IISER Kolkata) for spotting a numerical error in an earlier version. D.B. acknowledges support by the German Research Foundation (DFG), Grant ID BA 5847/2-1. The work of A.S. is partly supported through the Max Planck Partner Group between the Indian Association for the Cultivation of Science (Kolkata) and the Max Planck Institute for the Physics of Complex Systems (Dresden).

[1] J. M. Deutsch, Phys. Rev. A **43**, 2046 (1991).

[2] M. Srednicki, Phys. Rev. E **50**, 888 (1994).

[3] M. Rigol, V. Dunjko, and M. Olshanii, Nature **452**, 854

(2008).

- [4] A. Polkovnikov, K. Sengupta, A. Silva, and M. Vengalattore, Rev. Mod. Phys. **83**, 863 (2011).
- [5] L. D’Alessio, Y. Kafri, A. Polkovnikov, and M. Rigol, Advances in Physics **65**, 239 (2016).
- [6] P. Reimann, New Journal of Physics **17**, 055025 (2015).
- [7] C. Gogolin and J. Eisert, Rep. Prog. Phys. **79**, 056001 (2016).
- [8] L. Vidmar and M. Rigol, Journal of Statistical Mechanics: Theory and Experiment **2016**, 064007 (2016).
- [9] A. Pal and D. A. Huse, Phys. Rev. B **82**, 174411 (2010).
- [10] R. Nandkishore and D. A. Huse, Annu. Rev. Condens. Matter Phys. **6**, 15 (2015).
- [11] M. Brenes, M. Dalmonte, M. Heyl, and A. Scardicchio, Phys. Rev. Lett. **120**, 030601 (2018).
- [12] H. Bernien, S. Schwartz, A. Keesling, H. Levine, A. Omran, H. Pichler, S. Choi, A. S. Zibrov, M. Endres, M. Greiner, V. Vuletić, and M. D. Lukin, Nature **551**, 579 (2017).
- [13] C. J. Turner, A. A. Michailidis, D. A. Abanin, M. Serbyn, and Z. Papić, Nat. Phys. **14**, 745 (2018).
- [14] C. J. Turner, A. A. Michailidis, D. A. Abanin, M. Serbyn, and Z. Papić, Phys. Rev. B **98**, 155134 (2018).
- [15] P. Fendley, K. Sengupta, and S. Sachdev, Phys. Rev. B **69**, 075106 (2004).
- [16] I. Lesanovsky and H. Katsura, Phys. Rev. A **86**, 041601(R) (2012).
- [17] N. Shiraishi, J. Stat. Mech. (2019) 083103.
- [18] S. Moudgalya, N. Regnault, and B. A. Bernevig, Phys. Rev. B **98**, 235156 (2018).
- [19] S. Moudgalya, S. Rachel, B. A. Bernevig, and N. Regnault, Phys. Rev. B **98**, 235155 (2018).
- [20] D. K. Mark, C. -J. Lin, and O. I. Motrunich, Phys. Rev. B **101**, 195131 (2020).
- [21] S. Moudgalya, E. O’ Brien, B. A. Bernevig, P. Fendley, and N. Regnault, Phys. Rev. B **102**, 085120 (2020).
- [22] S. Moudgalya, B. A. Bernevig, and N. Regnault, Phys. Rev. B **102**, 195150 (2020).
- [23] B. Nachtergaele, S. Warzel, and A. Young, arXiv:2006.00300.
- [24] O. Vafek, N. Regnault, and B. A. Bernevig, SciPost Phys. **3**, 043 (2017).
- [25] T. Iadecola and M. Žnidarič, Phys. Rev. Lett. **123**, 036403 (2019).
- [26] D. K. Mark and O. I. Motrunich, Phys. Rev. B **102**, 075132 (2020).
- [27] S. Moudgalya, N. Regnault, and B. A. Bernevig, Phys. Rev. B **102**, 085140 (2020).
- [28] M. Schechter and T. Iadecola, Phys. Rev. Lett. **123**, 147201 (2019).
- [29] B. Mukherjee, S. Nandy, A. Sen, D. Sen, and K. Sengupta, Phys. Rev. B **101**, 245107 (2020).
- [30] S. Sugiura, T. Kuwahara, and K. Saito, arXiv:1911.06092.
- [31] S. Pai and M. Pretko, Phys. Rev. Lett. **123**, 136401 (2019).
- [32] B. Mukherjee, A. Sen, D. Sen, and K. Sengupta, Phys. Rev. B **102**, 014301 (2020).
- [33] B. Mukherjee, A. Sen, D. Sen, and K. Sengupta, Phys. Rev. B **102**, 075123 (2020).
- [34] H. Zhao, J. Vovrosh, F. Mintert, and J. Knolle, Phys. Rev. Lett. **124**, 160604 (2020).
- [35] K. Mizuta, K. Takasan, and N. Kawakami, Phys. Rev. Research **2**, 033284 (2020).

- [36] S. Ok, K. Choo, C. Mudry, C. Castelnovo, C. Chamon, and T. Neupert, Phys. Rev. Research **1**, 033144 (2019).
- [37] V. Khemani, M. Hermele, and R. Nandkishore, Phys. Rev. B **101**, 174204 (2020).
- [38] A. A. Michailidis, C. J. Turner, Z. Papić, D. A. Abanin, and M. Serbyn, Phys. Rev. Research **2**, 022065 (2020).
- [39] C. -J. Lin, V. Calvera, and T. H. Hsieh, Phys. Rev. B **101**, 220304(R) (2020).
- [40] K. Lee, R. Melendrez, A. Pal, and H. J. Changlani, Phys. Rev. B **101**, 241111(R) (2020).
- [41] P. A. McClarty, M. Haque, A. Sen, and J. Richter, Phys. Rev. B **102**, 224303 (2020).
- [42] Y. Kuno, T. Mizoguchi, and Y. Hatsugai, arXiv:2010.02044.
- [43] M. Serbyn, D. A. Abanin, Z. Papić, arXiv:2011.09486.
- [44] J. Kogut and L. Susskind, Phys. Rev. D **11**, 295 (1975).
- [45] F. M. Surace, P. P. Mazza, G. Giudici, A. Lerose, A. Gambassi, and M. Dalmonte, Phys. Rev. X **10**, 021041 (2020).
- [46] U. -J. Wiese, Annalen der Physik **525**, 777 (2013).
- [47] S. Chandrasekharan and U. -J. Wiese, Nuclear Physics B **492**, 455 (1997).
- [48] M. Hermele, M. P. A. Fisher, and L. Balents, Phys. Rev. B **69**, 064404 (2004).
- [49] N. Shannon, G. Misguich, and K. Penc, Phys. Rev. B **69**, 220403 (2004).
- [50] D. Banerjee, F.-J. Jiang, P. Widmer and U.-J. Wiese, J. Stat. Mech. P12010 (2013).
- [51] J. Villain, Z. Phys. B **33**, 31 (1979).
- [52] C. L. Henley, Phys. Rev. Lett. **62**, 2057 (1992).
- [53] J. -S. Bernier, M. J. Lawler, and Y. B. Kim, Phys. Rev. Lett. **101**, 047201 (2008).
- [54] P. A. McClarty, P. Stasiak, and M. J. P. Gingras, Phys. Rev. B **89**, 024425 (2014).
- [55] See Supplementary Material for more details on the exact diagonalization, calculation of bipartite entanglement entropy, level spacing distribution for the weakly disordered $U(1)$ QLM, Shannon entropy of energy eigenstates at $\lambda = 0$, momentum-resolved results for ladders of width $L_y = 4$ and finally, the QMBS expressed in terms of the zero modes.
- [56] Z. Lan and S. Powell, Phys. Rev. B **96**, 115140 (2017).
- [57] L. D' Alessio and M. Rigol, Phys. Rev. X **4**, 041048 (2014).
- [58] M. Schechter and T. Iadecola, Phys. Rev. B **98**, 035139 (2018).
- [59] R. Jackiw and C. Rebbi, Phys. Rev. D **13**, 3398 (1976).
- [60] W. P. Su, J. R. Schrieffer, and A. J. Heeger, Phys. Rev. Lett. **42**, 1698 (1979).
- [61] R. Jackiw and P. Rossi, Nucl. Phys. B **190**, 681 (1981).
- [62] E. J. Weinberg, Phys. Rev. D **24**, 2669 (1981).
- [63] J. C. Y. Teo and C. L. Kane, Phys. Rev. B **82**, 115120 (2010).
- [64] E. Witten, Nucl. Phys. B **188**, 513 (1981).
- [65] D. Marcos, P. Widmer, E. Rico, M. Hafezi, P. Rabl, U.-J. Wiese, P. Zoller, Annals Phys. **351**, 634 (2014).
- [66] A. Celi, B. Vermersch, O. Viyuela, H. Pichler, M. D. Lukin, P. Zoller, Phys. Rev. X **10**, 021057 (2020).

**SUPPLEMENTARY MATERIAL FOR
“QUANTUM SCARS FROM ZERO MODES IN
AN ABELIAN LATTICE GAUGE THEORY ON
LADDERS”**

ASPECTS OF EXACT DIAGONALIZATION

(L_x, L_y)	Gauss law	$(W_x, W_y) = (0, 0)$	$(k_x, k_y) = (0, 0)$
(8, 2)	7074	2214	142
(10, 2)	61098	17906	902
(12, 2)	539634	147578	6166
(14, 2)	4815738	1232454	44046
(16, 2)	43177794	10393254	324862
(4, 4)	2970	990	70
(6, 4)	98466	32810	1384
(8, 4)	3500970	1159166	36360
(6, 6)	16448400	5482716	152416

The unconstrained Hamiltonian with $S = 1/2$ links on a (L_x, L_y) ladder contains $2^{2L_x L_y}$ configurations. Since gauge-invariant states have the added constraint that in- and out-going electric fluxes add up to zero at each site, this dramatically decreases the number of allowed states in the Hilbert space. Furthermore, restricting to the largest topological sector with $(W_x, W_y) = (0, 0)$ reduces the number of allowed configurations even further. Lastly, using the additional global symmetries of translations in both directions, allows access to bigger system sizes as shown in the table for the largest momentum block of $(k_x, k_y) = (0, 0)$ for various (L_x, L_y) . We are able to obtain the full spectrum of Hamiltonians with upto ~ 75000 states, while real-time dynamics is possible for Hamiltonians with upto ~ 50000 states.

**CALCULATION OF BIPARTITE
ENTANGLEMENT ENTROPY**

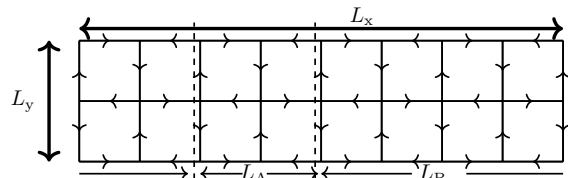


FIG. 6: A ladder of dimension (L_x, L_y) is divided into two subsystems of dimensions L_A and L_B along its length for calculating the bipartite entanglement entropy.

We outline computation for the bipartite entanglement entropy in the ladder geometry (L_x, L_y) . Let n_D denote the total of gauge invariant basis states in a given sector

(W_x, W_y) , where we represent the basis as:

$$\{|e\rangle\} = \{|e_k\rangle; k = 1, \dots, n_D\}, \quad (2)$$

and a wavefunction in this sector can be written as a linear superposition

$$|\psi\rangle = \sum_{k=1}^{n_D} c_k |e_k\rangle. \quad (3)$$

To compute the bipartite entanglement entropy S_A for the partition of the system into two subsystems, as sketched in Fig 6, we first denote the basis states spanning the two partitions by $\{|e^{(A)}\rangle\}$ and $\{|e^{(B)}\rangle\}$. Note that $\{|e^{(A,B)}\rangle\}$ are gauge invariant at all points in the bulk regions A and B respectively, but represent surface charges at the boundaries.

The calculation of $\{|e^{(A,B)}\rangle\}$ is straightforward: for each k in $\{|e_k\rangle\}$, we split the links along the vertical dotted line shown in the figure and sort them into $\{|e^{(A)}\rangle\}$ and $\{|e^{(B)}\rangle\}$ respectively, depending on whether they fall into the region A or B. Then, we remove the duplicates and obtain:

$$\begin{aligned} \{|e^{(A)}\rangle\} &= \{|e_{i_A}^{(A)}\rangle, i_A = 1, \dots, D_A\} \\ \{|e^{(B)}\rangle\} &= \{|e_{i_B}^{(B)}\rangle, i_B = 1, \dots, D_B\} \end{aligned} \quad (4)$$

Now, for a general energy eigenstate $|\psi\rangle$,

$$\begin{aligned} |\psi\rangle &= \sum_k^{n_D} c_k |e_k\rangle \\ &= \sum_{i_A}^{D_A} \sum_{i_B}^{D_B} \chi_{i_A, i_B} |e_{i_A}^{(A)}\rangle \otimes |e_{i_B}^{(B)}\rangle \\ &= \sum_{\ell}^{n_\chi} \chi_{\ell} |\tilde{e}_{\ell}^{(A)}\rangle \otimes |\tilde{e}_{\ell}^{(B)}\rangle \end{aligned} \quad (5)$$

First, the individual basis vectors from the two subsystems are "patched" with each other: for example the i_A from $|e^{(A)}\rangle$ is patched with i_B from $|e^{(B)}\rangle$ to form the corresponding matrix element $\chi(i_A, i_B)$. Clearly, this makes χ a rectangular matrix of dimensions $D_A \times D_B$. To go from the second to the third step, one does Schmidt decomposition, which yield the real and non-negative Schmidt values $\chi_{\ell}, \ell = 1, \dots, n_{\chi}$, where $n_{\chi} = \min(D_A, D_B)$.

The (von-Neumann) entanglement entropy for this sub-partition of the state $|\psi\rangle$ when $L_A = L_B$ then given by

$$S_{L/2} = - \sum_{i=1}^{n_{\chi}} |\chi_i|^2 \ln(|\chi_i|^2) \quad (6)$$

and is shown in the main text.

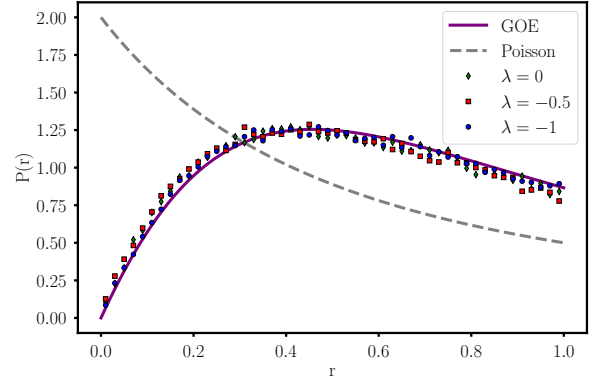


FIG. 7: The probability distribution, $P(r)$, obtained from the ratio of consecutive energy gaps for the weakly disordered $U(1)$ QLM on a ladder of dimension $(L_x, L_y) = (12, 2)$ for $\lambda = 0, -0.5, -1.0$ matches well with the prediction from the Gaussian orthogonal ensemble (thick curve), and not the Poisson statistics expected for integrable systems (dotted curve).

LEVEL SPACING DISTRIBUTION FOR WEAKLY DISORDERED $U(1)$ QLM

To show that the $U(1)$ QLM on ladders is non-integrable in the topological sector $(W_x, W_y) = (0, 0)$, we take a ladder of dimension $(L_x, L_y) = (12, 2)$ and weakly disorder the λ term in Eq. 1 of main text to $\lambda_i = \lambda(1 + \alpha r_i)$ ($\lambda_i = \alpha r_i$) for non-zero (zero) λ where $\alpha = 0.1$ and r_i is a random number chosen with uniform probability between $[-1/2, 1/2]$ on the i th elementary plaquette. The small α ensures that the global symmetries of translations and point-group symmetries of reflections and 180° rotations are lifted. We then resolve the energy eigenstates in the only remaining (internal) symmetry of charge conjugation and focus on the block with eigenvalue of $+1$ (the other block has eigenvalue -1) which gives 73789 energy eigenvalues (denoted by E_n). We then obtain the probability distribution $P(r)$, with r being the ratio of two consecutive energy gaps,

$$\begin{aligned} r &= \frac{\min(s_n, s_{n+1})}{\max(s_n, s_{n+1})} \in [0, 1] \\ s_n &= E_{n+1} - E_n \end{aligned} \quad (7)$$

For a system satisfying ETH, this distribution is expected to converge to the Gaussian orthogonal ensemble, where

$$P_{GOE}(r) = \frac{27}{4} \frac{r + r^2}{(1 + r + r^2)^{5/2}}. \quad (8)$$

This indeed seems to be the case for the weakly disordered $U(1)$ QLM for $\lambda = 0, -0.5, -1.0$ (Fig. 7). On the other hand, the level statistics for an integrable system should follow Poisson statistics with $P(r) = 2/(1+r)^2$ (also shown for reference in Fig. 7).

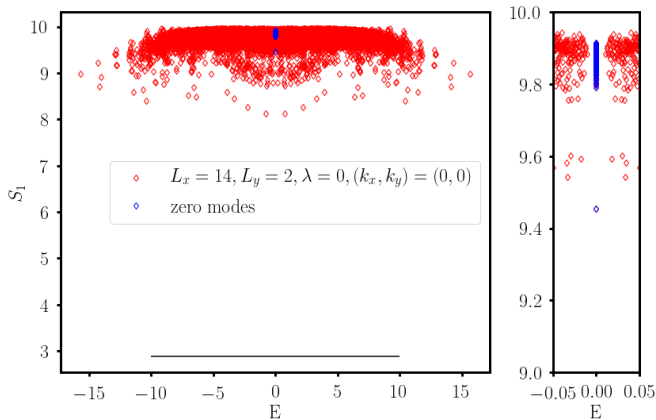


FIG. 8: (Left panel) The behavior of Shannon entropy, S_1 , for the energy eigenstates with momentum $(k_x, k_y) = (0, 0)$ shown at coupling $\lambda = 0$ for ladder dimension of $(L_x, L_y) = (14, 2)$. The horizontal line equals the value of S_1 for the QMBS at finite λ . (Right panel) The same data of S_1 shown in the vicinity of $E = 0$. The zero modes are indicated in blue for both panels.

SHANNON ENTROPY OF ENERGY EIGENSTATES AT $\lambda = 0$

The Shannon entropy, S_1 , of the energy eigenstates at $\lambda = 0$ with momentum $(k_x, k_y) = (0, 0)$ is shown in Fig. 8 (left panel) for a ladder of dimension $(L_x, L_y) = (14, 2)$. The S_1 for the QMBS at $\lambda \neq 0$ is also shown as a horizontal line from which it is clear that the QMBS is much more localized in the Hilbert space. Fig. 8 (right panel) shows the same data for S_1 at $\lambda = 0$ in the vicinity of $E = 0$ with the zero modes indicated in blue, which shows that the zero modes are as delocalized in the Hilbert space as the non-zero modes in the neighborhood and do not have an anomalously low S_1 like the QMBS (that emerges at finite λ).

QMBS FOR $(k_x, k_y) = (0, 0), (\pi, \pi), (\pi, 0), (0, \pi)$ FOR LADDERS OF WIDTH $(L_x, L_y) = (8, 4)$

Unlike the case of $L_y = 2$ where the ladders have 4 QMBS, one each at momenta $(k_x, k_y) = (0, 0), (\pi, \pi), (\pi, 0), (0, \pi)$, the wider ladder of width $L_y = 4$ have multiple scars at each of these four momenta (10 for $(k_x, k_y) = (0, 0)$ and (π, π) respectively and 9 for $(k_x, k_y) = (\pi, 0)$ and $(0, \pi)$ respectively). This is seen clearly from the behavior of the Shannon entropy S_1 (Fig. 9, top left panel) and the electric flux correlator (Fig. 9, bottom panel) for a ladder of dimension $(L_x, L_y) = (8, 4)$ at $\lambda = -1$ where the data shows outliers at $E = \lambda N_p/2$. As shown in Fig. 9 (top right panel) for $(k_x, k_y) = (0, 0)$, these 10 scars are degenerate with energy $\lambda N_p/2$ and have a lower value of S_1 compared to that of other neighboring eigenstates with $E \neq \lambda N_p/2$.

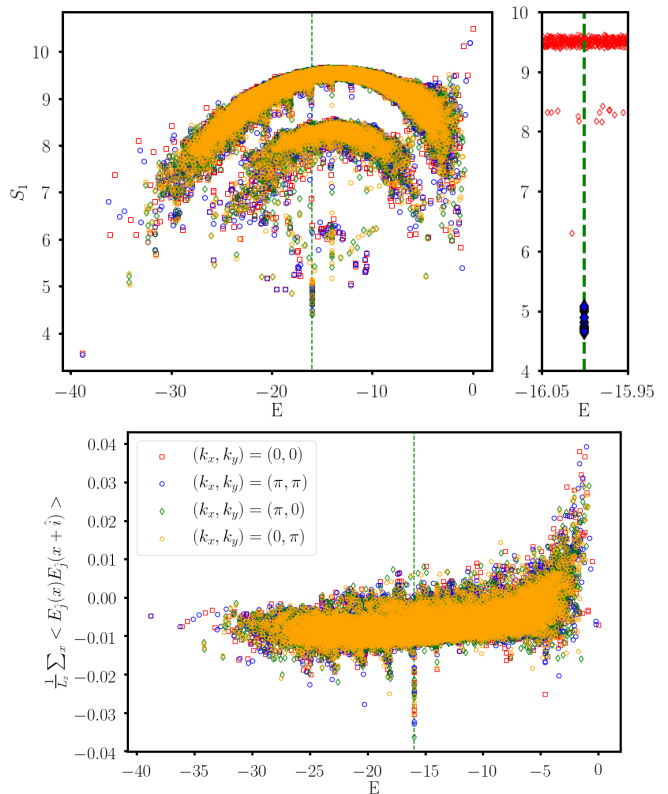


FIG. 9: The Shannon entropy, S_1 , (top left panel) and the electric flux correlator (bottom panel) for all energy eigenstates of $(L_x, L_y) = (8, 4)$ at $(W_x, W_y) = (0, 0)$, and for the momenta $(k_x, k_y) = (0, 0), (\pi, \pi), (\pi, 0), (0, \pi)$ (shown in red, blue, green, orange) with coupling $\lambda = -1$. The top right panel shows the same data for S_1 for $(k_x, k_y) = (0, 0)$ in the vicinity of $\lambda N_p/2$.

QMBS FROM ZERO MODES

The QMBS at momentum $(k_x, k_y) = (0, 0)$ obtained at $\lambda \neq 0$ for the ladder of dimension $(L_x, L_y) = (14, 2)$ is a very particular linear combination of the mid-spectrum zero modes at $\lambda = 0$ that also diagonalizes \mathcal{O}_{pot} . However, from Fig. 10 (top panel), the QMBS appears to be a pseudo-random superposition of all the zero modes which is, remarkably, stabilized at any finite λ . We have also verified that the matrix for \mathcal{O}_{pot} , when expressed in the basis of the zero modes at momentum $(k_x, k_y) = (0, 0)$, has a single eigenvalue which is an integer (that equals $N_p/2$). This wavefunction (Fig. 10 (bottom panel)) is identical to the one obtained directly from the ED data for the $(k_x, k_y) = (0, 0)$ QMBS at $\lambda = -1$ (Fig. 10 (middle panel)). Only 18 out of the 44046 basis states have non-zero coefficients while the other coefficients are (essentially) zero within numerical resolution. The number of basis states that contribute to the QMBS at momenta $(0, 0), (\pi, \pi), (\pi, 0), (0, \pi)$ for $(L_x, 2)$ with $8 \leq L_x \leq 14$ is given below. The table immediately shows that these

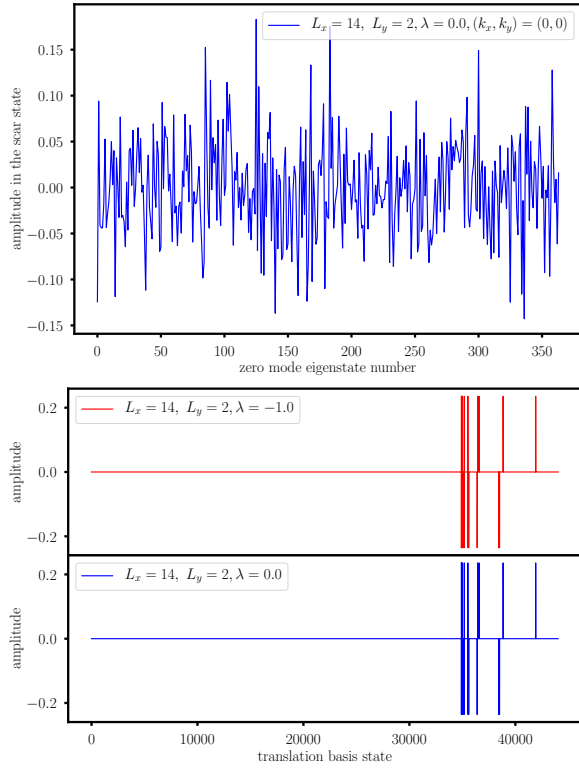


FIG. 10: (Top panel) The QMBS at momentum $(k_x, k_y) = (0, 0)$ expressed in terms of the zero modes for a ladder of dimension $(L_x, L_y) = (14, 2)$. The amplitude of the QMBS expressed in the basis states of momentum $(k_x, k_y) = (0, 0)$ where the the middle plot is directly obtained from the wavefunction of the QMBS at $\lambda = -1$ while the bottom plot is obtained from the eigenvector with integer eigenvalue of \mathcal{O}_{pot} in the subspace of the zero modes at $\lambda = 0$.

eigenstates are localized in the Hilbert space and have a low value of Shannon entropy S_1 .

L_x	Basis states in $(0, 0)/(\pi, \pi)$	Basis states in QMBS	Basis states in $(\pi, 0)/(0, \pi)$	Basis states in QMBS
8	142	5	141	4
10	902	6	891	7
12	6166	13	6163	12
14	44046	18	43989	19